

Role of Arg100 and Arg264 from *Anabaena* PCC 7119 Ferredoxin–NADP⁺ Reductase for Optimal NADP⁺ Binding and Electron Transfer[†]

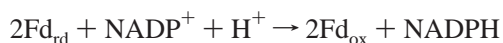
Marta Martínez-Júlvez,[‡] Juan Hermoso,[§] John K. Hurley,^{||} Tomás Mayoral,[§] Julia Sanz-Aparicio,[§] Gordon Tollin,^{||} Carlos Gómez-Moreno,[‡] and Milagros Medina^{*,‡}

Departamento de Bioquímica y Biología Molecular y Celular, Facultad de Ciencias, Universidad de Zaragoza, 50009 Zaragoza, Spain, Grupo de Cristalografía Macromolecular y Biología Estructural, Instituto Química-Física Rocasolano, CSIC, Serrano 119, 28006 Madrid, Spain, and Department of Biochemistry, University of Arizona, Tucson, Arizona 85721

Received July 16, 1998; Revised Manuscript Received October 13, 1998

ABSTRACT: Previous studies and the crystal structure of *Anabaena* PCC 7119 FNR suggest that the side chains of Arg100 and Arg264 may be directly involved in the proper NADP⁺/NADPH orientation for an efficient electron-transfer reaction. Protein engineering on Arg100 and Arg264 from *Anabaena* PCC 7119 FNR has been carried out to investigate their roles in complex formation and electron transfer to NADP⁺ and to ferredoxin/ferredoxin. Arg100 has been replaced with an alanine, which removes the positive charge, the long side chain, as well as the ability to form hydrogen bonds, while a charge reversal mutation has been made at Arg264 by replacing it with a glutamic acid. Results with various spectroscopic techniques indicate that the mutated proteins folded properly and that significant protein structural rearrangements did not occur. Both mutants have been kinetically characterized by steady-state as well as fast transient kinetic techniques, and the three-dimensional structure of Arg264Glu FNR has been solved. The results reported herein reveal important conceptual information about the interaction of FNR with its substrates. A critical role is confirmed for the long, positively charged side chain of Arg100. Studies on the Arg264Glu FNR mutant demonstrate that the Arg264 side chain is not critical for the nicotinamide orientation or for nicotinamide interaction with the isoalloxazine FAD moiety. However, this mutant showed altered behavior in its interaction and electron transfer with its protein partners, ferredoxin and flavodoxin.

Ferredoxin–NADP⁺ reductase (FNR,¹ EC 1.18.1.12) is a flavoenzyme which catalyzes NADPH formation during photosynthesis, according to the reaction (1)



The three-dimensional structure of this enzyme has been shown to be the prototype of a large family of flavin-dependent oxidoreductases that function as transducers between nicotinamide dinucleotides (two-electron carriers) and various one-electron carriers (2–4). The three-dimensional structures of oxidized and reduced native spinach FNR

and that of a complex with 2'-phospho-5'-AMP have been reported (2). The three-dimensional structure of *Anabaena* FNR and that of a complex with NADP⁺ have also been determined (5).

The electron-transfer reactions between *Anabaena* PCC 7119 FNR and its physiological partners have been extensively studied (6–15). When this organism is grown under low-iron conditions, flavodoxin is synthesized instead of ferredoxin, and replaces it in the electron-transfer reaction from PSI to FNR (16). The three-dimensional structure of *Anabaena* FNR resembles that of the spinach enzyme and consists of two different domains (4, 5). The FAD binding domain is made up of a scaffold of six antiparallel strands arranged in two perpendicular β -sheets, the bottom of which is capped by a short α -helix and a long loop. The NADP⁺ binding domain consists of a core of five parallel β -strands surrounded by six α -helices. The edge of the dimethylbenzene ring of FAD, which is the only part of the flavin isoalloxazine moiety exposed to the solvent, is putatively involved in intermolecular electron transfer with ferredoxin or flavodoxin.

Chemical modification studies have implicated Arg224, Lys227, and Arg233 (12, 13) in the *Anabaena* FNR and Lys116 and Lys244 (corresponding to Arg100 and Arg233 in the *Anabaena* enzyme) (17–19) in the spinach enzyme in the interaction with the NADP⁺ cofactor. The role of the side chain of Lys116 in catalysis in the spinach FNR has been probed by replacement of this residue by a glutamine

[†] This work was supported by the Comisión Interministerial de Ciencia y Tecnología (Grant BIO-94-0621-C02-01 to C.G.-M.) and the National Institutes of Health (Grant DK15057 to G.T.).

* To whom correspondence should be addressed: Departamento de Bioquímica y Biología Molecular y Celular, Facultad de Ciencias, Universidad de Zaragoza, 50009 Zaragoza, Spain. Phone: 34 976 761279. Fax: 34 976 762123. E-mail: mmedina@posta.unizar.es.

[‡] Universidad de Zaragoza.

[§] Instituto Química-Física Rocasolano, CSIC.

^{||} University of Arizona.

¹ Abbreviations: FNR, ferredoxin–NADP⁺ reductase; FNR_{ox}, FNR in the oxidized state; FNR_{rd}, FNR in the reduced state; FNR_{sq}, FNR in the semiquinone state; Fd, ferredoxin; Fd_{ox}, Fd in the oxidized state; Fd_{rd}, Fd in the reduced state; Fld, flavodoxin; Fld_{ox}, Fld in the oxidized state; Fld_{sq}, Fld in the semiquinone state; Fld_{rd}, Fld in the reduced state; IPTG, isopropyl β -D-thiogalactoside; dRf, 5-deazariboflavin; dRfH⁺, semiquinone form of dRf; DCPIP, 2,6-dichlorophenolindophenol; et, electron transfer; PDR, phthalate dioxygenase reductase; PSI, photosystem I.

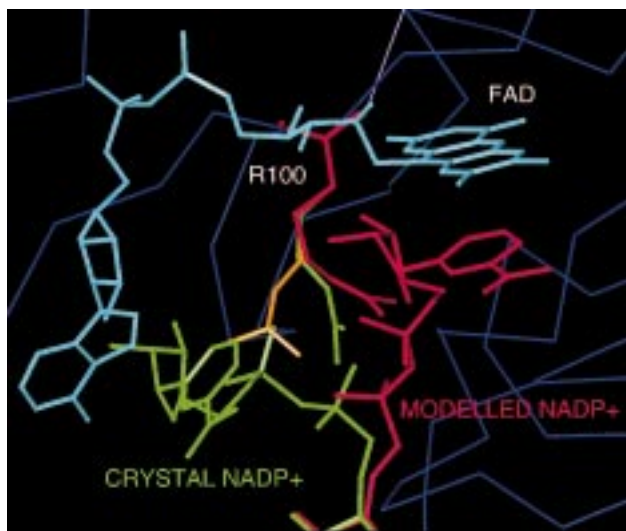


FIGURE 1: Different orientations of Arg100 in wild-type FNR (orange), in the crystallographic NADP⁺-FNR complex (green), and in the modeled NADP⁺-FNR complex (red). This figure was generated with the O graphics program (40).

using site-directed mutagenesis (20). The three-dimensional structure obtained for a complex of *Anabaena* FNR and NADP⁺ confirmed most of the observations of that study (5). The adenine ring of NADP⁺ interacts through hydrogen bonding with Gln237 and is stacked with the Tyr235 side chain. The 2'-phosphate interacts with Ser223, Arg224, Arg233, and Tyr235, and the adenine 5'-phosphoryl is hydrogen bonded to Arg100. However, in this FNR-NADP⁺ complex, the nicotinamide ring is turned toward the FNR molecular surface and does not stack onto the FAD isoalloxazine ring as would be required for hydride and proton transfer (5). The side chains of several residues (Arg100, Arg224, Arg233, Tyr235, Gln237, and Glu103) are displaced by the presence of substrate in the complex. In particular, movement of Arg100 is detected upon NADP⁺ binding which seems to interfere with the binding of the nicotinamide ring. In these FNR-soaked crystals, the NADP⁺ position seems to be only partially occupied and two weak electron density positions for Arg100 indicate an alternate position for this residue (Figure 1). One position corresponds to that found in the free enzyme, while in the other position, Arg100 interacts with the pyrophosphate bridge of NADP⁺ which causes it to lie on the surface of the protein in such a manner that no hydride exchange is possible between N5 of the FAD isoalloxazine and C4 of the nicotinamide (5). The observed binding is presumed to represent an alternative mode of interaction between the oxidized pyridine nucleotide and the oxidized enzyme. It is apparently unfavorable for the positively charged oxidized nicotinamide ring to be buried in the nicotinamide pocket, the most likely reason for this being an unfavorable electrostatic interaction with the guanidinium group of Arg100. A similar situation has been described for the binding of NADP⁺ to glutathione reductase, whereas no problem was detected in the binding of NADPH (21). An "ideal" model for NADP⁺ binding has been constructed on the basis of the NADP⁺-bound structure and the fact that during catalysis the nicotinamide ring must stack against the FAD isoalloxazine ring (5). A third position for the Arg100 side chain is proposed in this model (Figure 1). Two possibilities also exist for the nicotinamide stacking

against the isoalloxazine ring. The nicotinamide ring could be sandwiched between the aromatic ring of the terminal Tyr303 and the isoalloxazine ring, as in glutathione reductase or in NAD(P)H quinone reductase (21, 22). An alternative mechanism has also been proposed involving an additional movement of the aromatic ring of Tyr303, with stabilization being provided by stacking with the guanidinium moiety of Arg264 and the stacking of the nicotinamide moiety with the isoalloxazine. Moreover, Arg264 may play an additional role in ferredoxin recognition (5, 23).

Sequence comparisons of *Anabaena* PCC 7119 with FNRs from different sources and with other members of the FNR family are shown in Table 1. Both Arg100 and Arg264 are conserved as positively charged residues in all the FNR sequences analyzed thus far, but not in other family members, indicating that although its function is well-conserved in the FNRs, it is not conserved in other family members. In this study, protein engineering on Arg100 and Arg264 of *Anabaena* PCC 7119 FNR has been carried out to investigate their roles in complex formation and electron transfer to NADP⁺ and to ferredoxin/ferredoxin. Removal of these positively charged residues might be expected to produce significant changes in complex stabilization between FNR and its cofactors. Arg100 has been replaced by an alanine, which removes the positive charge, the long side chain, as well as the ability to make hydrogen bonds, while a charge-reversal mutation has been constructed at Arg264 by replacing it with a glutamic acid.

MATERIALS AND METHODS

Oligonucleotide-Directed Mutagenesis. Mutations of recombinant *Anabaena* PCC 7119 FNR at Arg100 and Arg264 were carried out using the Transformer site-directed mutagenesis kit from Clontech in combination with the synthetic oligonucleotides 5' TA GTG TAA TTG GCA GAG GGA GAG 3' for Arg100Ala and 5' CTC TTC CAT ACC CTC CAA ACC ACA GAT G 3' for Arg264Glu and the trans oligo *Nde*I-*Sac*II 5' AGT GCA CCA TCC GCG GTG TGA 3'. As template, a construct of the *petH* gene (24) which has been previously cloned into the expression plasmid pTrc99a (25) was used. Mutations were verified by DNA sequence analysis. The constructs containing the mutated FNR gene were used to transform the *Escherichia coli* PC 0225 strain (25).

Purification of Proteins. *Anabaena* PCC 7119 Arg100Ala and Arg264Glu FNR mutants were purified from IPTG-induced cultures as previously described (11, 25). Recombinant ferredoxin and flavodoxin from *Anabaena* were also prepared as described previously (9, 26). UV-visible spectra and SDS-PAGE were used as purity criteria.

Spectral Analysis. UV-visible spectra were measured on a Cary-15 (Olis-modified), a Hewlett-Packard 8452 diode array, or a Kontron Uvikon 942 spectrophotometer. Circular dichroism (CD) spectra were obtained using a Jasco 710 spectropolarimeter at room temperature in a 1 cm path length cuvette. For the CD measurements, protein concentrations were 4 μ M for the visible and aromatic regions of the spectrum and 0.7 μ M for the far-UV regions. Samples were prepared in 1 mM Tris-HCl (pH 8.0). Protein and flavin fluorescence were measured using a Kontron SFM 25 spectrofluorometer interfaced with a PC computer. Solutions

Table 1: Conservation of the Arg100 and Arg264 Residues of *Anabaena* PCC 7119 in the FNR Family^a

FNRs	95	103	260	270	Reference
<i>Anabaena</i> PCC 7119	I S L C V R Q L E		I C G L R G M E E G I		(44)
<i>Spirulina</i> sp	V * * * * * * * *		* * * * K * * * G * *		(45)
Spinach	V * * * * K R * I		M * * * K * * * K * *		(4)
<i>M. crystallinum</i>	V * * * * K R * I		M * * * K * * * K * *		(46)
<i>P. sativum</i>	V * * * * K R * V		M * * * K * * * K * *		(47)
<i>C. paradoxa</i>	V * * S * K R * *		M * * * * * * * D * *		(48)
<i>Synechococcus</i> 7002	V * * * * * * * *		M * * * K * * * Q P P *		(49)
Other reductases of the FNR family					
Rat liver cytochrome P450 reductase	V H I C A V A V E		V * * - K D V Q N T F		(50)
<i>Salmonella typhimurium</i> Sulphite reductase	V H I T * G V V R		V * * A A D V E K A L		(51)
Human erythrocytes cytochrome b ₅ reductase	* K V Y F K D T H		M * * P P P * I Q Y A		(52)
<i>Pseudomonas cepacia</i> PDR	Y V I A * K R D S		C * * P Q A L M D T V		(53)

^a The final alignments were obtained by visual inspection. Asterisks indicate exact matches of the sequences to that of *Anabaena* PCC 7119 FNR. The hyphen represents an amino acid deletion.

used for fluorescence spectra contained 4 μ M protein in 50 mM Tris-HCl (pH 8.0).

Binding Constants. Dissociation constants and binding energies of the complexes between oxidized FNR species and NADP⁺, oxidized ferredoxin, or oxidized flavodoxin were obtained as previously described (11, 15). The experiments were performed on solutions containing approximately 30 μ M FNR in 50 mM Tris-HCl buffer (pH 8.0) at 25 °C, into which aliquots of concentrated ligand were added.

Enzymatic Assays. The diaphorase activity, with DCPIP as the electron acceptor, and the FNR-dependent NADPH-cytochrome *c* reductase activity, using either ferredoxin or flavodoxin, were measured as described previously (11, 27, 28). The standard reaction mixtures contained varied concentrations of NADPH, ferredoxin, or flavodoxin for calculating the corresponding K_m values. All the measurements were carried out at 25 °C in 50 mM Tris-HCl (pH 8.0), unless otherwise stated.

FNR Photoreduction. Photoreduction of protein-bound flavin was performed under anaerobic conditions in the presence of EDTA and 5-deazariboflavin as previously described (11).

Laser Flash Photolysis Measurements. The laser flash photolysis apparatus and the experimental protocol have been described previously (9, 11, 29). In the current system, the Nicolet 1170 signal averager has been replaced by a Tektronix TDS410A digitizing oscilloscope. The mechanism by which 5-deazariboflavin (dRf) initiates protein-protein electron transfer has also been described previously (30). Digitized kinetic traces were analyzed using a computer fitting routine (Kinfit, Olis Co., Bogart, GA). Generally, four to ten flashes were averaged. Experiments were carried out under pseudo-first-order conditions in which Fd is present in large excess over the dRf* generated by the laser flash (<1 μ M). Laser flash-induced kinetic measurements were taken at room temperature. In addition to protein, samples

also contained 1 mM EDTA and 95–100 μ M dRf in 4 mM potassium phosphate buffer (pH 7.0). The ionic strength of the solution was adjusted using a 5 M NaCl stock solution. Samples were made anaerobic as described previously (11, 31).

The kinetic data shown in Figures 2 and 3 were taken at 600 nm, a wavelength at which the production of FNR_{sq} can be monitored as FNR_{ox} is reduced by Fd_{rd}. Data collected at 507 nm, a wavelength at which the oxidation of Fd_{rd} can be monitored, yielded rate constants that were the same, within experimental error, as those determined from the 600 nm data, as expected from the following simple (minimal) two-step mechanism (eq 1)



Binding constants for the intermediate Fd_{rd}-FNR_{ox} complexes and electron-transfer rate constant values were determined by fitting the laser flash photolysis kinetic data (Figure 2A) to the exact solution of the differential equation describing the minimal (two-step) mechanism (eq 1) (32, 33).

Estimation of Reduction Potentials. Reduction potentials for the oxidized/semiquinone couples (E°) of the FNR mutants were estimated by comparison of the extent of reoxidation of Fd_{rd} by FNR_{ox} observed at 507 nm in the laser flash photolysis measurements relative to the extent of reoxidation produced using wild-type FNR under comparable conditions.

Stopped-Flow Measurements. Electron-transfer processes between FNR and its substrates (NADP⁺/NADPH, Fd, or Fld) were studied using stopped-flow methodology under anaerobic conditions using an Applied Photophysics SX17.MV spectrophotometer interfaced with an Acorn 5000 computer using the SX.17MV software of Applied Photophysics as previously described (11). The observed rate constants (k_{obs})

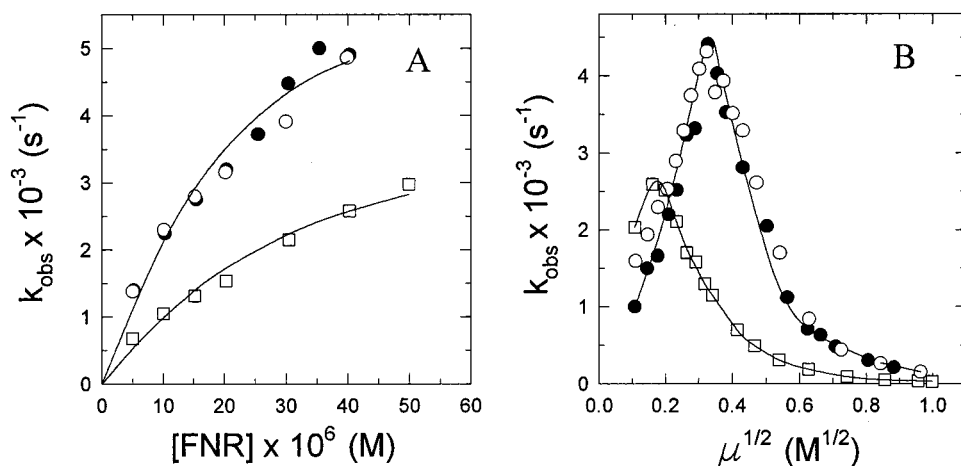


FIGURE 2: (A) FNR concentration dependence for the reduction of wild-type (●), Arg100Ala (○), and Arg264Glu (□) FNR species by Fd_{rd} at an ionic strength of 100 mM. For the wild-type and Arg100Ala experiments, FNR was titrated into 40 μM Fd. For the Arg264Glu experiment, FNR was titrated into 30 μM Fd. Solid lines through the data represent theoretical fits assuming a two-step mechanism (see the text for details). The fit to the Arg100Ala data can almost be superimposed with that of the wild-type data and is not shown. (B) Ionic strength dependence of k_{obs} for the reduction of wild-type (●), Arg100Ala (○), and Arg264Glu (□) FNR forms by Fd_{rd}. The k_{obs} values have been normalized to 30 μM FNR. The actual FNR concentrations were 30 μM for the wild-type reaction and 40 μM for the experiments with the mutants. All experimental mixtures contained 40 μM Fd. The ionic strength was adjusted using aliquots of 5 M NaCl. Deaerated solutions also contained 95–100 μM dRf and 1 mM EDTA in 4 mM potassium phosphate buffer (pH 7.0).

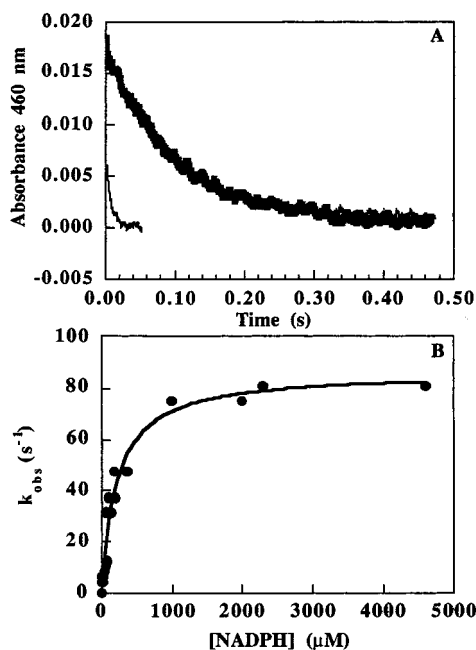


FIGURE 3: (A) Time course of anaerobic reduction of FNR species by NADPH. Final concentrations after mixing were as follows: 5 μM wild-type FNR_{ox} (narrow trace) was reacted with 44 μM NADPH, and 6.5 μM Arg100Ala FNR_{ox} (wide trace) was reacted with 40 μM NADPH. The monitoring wavelength was 460 nm. (B) NADPH concentration dependence of the observed rate constants for Arg100Ala FNR_{ox} reduction. Reactions were carried out in 50 mM Tris-HCl (pH 8.0) at 13 °C.

were calculated by fitting the data to a mono- or biexponential equation. The measurement of the reoxidation rate of the different reduced FNR forms by molecular O₂ was carried out using an air-saturated 50 mM Tris-HCl solution (pH 8.0).

Reactant concentrations for the stopped-flow experiments were as follows (final concentrations): 5 μM wild-type FNR_{ox}, 6.5 μM Arg100Ala FNR_{ox}, and 10 μM Arg264Glu FNR_{ox} were reacted with 44, 40, and 40 μM NADPH, respectively; 7.5 μM wild-type FNR_{rd}, 10 μM Arg100Ala

FNR_{rd}, and 9.2 μM Arg264Glu FNR_{rd} were reacted with 44, 50, and 39 μM NADP⁺, respectively; 9.5 μM wild-type FNR_{ox}, 9 μM Arg100Ala FNR_{ox}, and 10 μM Arg264Glu FNR_{ox} were reacted with 28, 25, and 23 μM Fd_{rd}, respectively; 7 μM wild-type FNR_{rd}, 6 μM Arg100Ala FNR_{rd}, and 8.75 μM Arg264Glu FNR_{rd} were reacted with 22, 20, and 24 μM Fd_{ox}, respectively; 10 μM wild-type FNR_{ox}, 9 μM Arg100Ala FNR_{ox}, and 12 μM Arg264Glu FNR_{ox} were reacted with 24, 22, and 26 μM Fld_{rd}, respectively; 11.5 μM wild-type FNR_{rd}, 15 μM Arg100Ala FNR_{rd}, and 9 μM Arg264Glu FNR_{rd} were reacted with 27.5, 27, and 26 μM Fld_{ox}, respectively; and 8.5 μM wild-type FNR_{rd}, 9 μM Arg100Ala FNR_{rd}, and 9 μM Arg264Glu FNR_{rd} were reacted with an air-saturated 50 mM Tris-HCl solution (pH 8.0).

Crystal Growth, Data Collection, and Structure Refinement. Crystals of Arg264Glu FNR were grown by the hanging drop method. The 5 μL droplets consisted of 2 μL of a 25.9 mg of protein/mL solution buffered with 10 mM Tris-HCl (pH 8), 1 μL of unbuffered β-octyl glucoside at 5% (w/v), and 2 μL of reservoir solution containing 17% (w/v) poly(ethylene glycol) (PEG) 6000, 20 mM ammonium sulfate, and 0.1 M MES (pH 4.9). The droplet was equilibrated against 1 mL of reservoir solution at 20 °C. Under these conditions, crystals grew, within 1–7 days, up to a maximum size of 0.8 mm × 0.4 mm × 0.4 mm in the presence of phase separation caused by the detergent.

X-ray data for the Arg264Glu FNR were collected at 20 °C to 2.3 Å resolution on a Mar-Research Image Plate detector using graphite-monochromated CuKα radiation generated by an Enraf-Nonius rotating anode generator operating at 35 kV and 99 mA. Crystals belong to the P6₅ hexagonal space group with the following unit cell dimensions: $a = b = 88.09$ Å and $c = 97.21$ Å. The V_M is 3.0 Å³/Da (34) with one FNR molecule in the asymmetric unit and 60% solvent content. The X-ray data set was processed with MOSFLM (35) and scaled and reduced with SCALA, from the CCP4 package (36). The Arg264Glu structure was solved by molecular replacement using the program AMoRe (37) on the basis of the 1.8 Å resolution native FNR model

Table 2: Refinement Statistics

σ cutoff	none
resolution range (Å)	9.0–2.3
no. of reflections used	18504
no. of protein atoms	2336
no. of ligand atoms	58
no. of solvent atoms	332
<i>R</i> factor ^a	0.16
free <i>R</i> factor	0.22
rms deviation	
bond lengths (Å)	0.007
bond angles (deg)	1.21
dihedrals	26.17
impropers	1.55
Ramachandran outliers	none

$$^a R \text{ factor} = \frac{\sum(|F_o| - |F_c|)}{\sum|F_o|}$$

(5) without the FAD cofactor. An unambiguous single solution for the rotation and translation functions was obtained. This solution was refined by the fast rigid-body refinement program FITING (38). The model was subjected to alternate cycles of conjugate gradient refinement with the program X-PLOR (39) and manual model building with the software package O (40). The crystallographic *R* and *R*_{free} values converged to values of 0.16 and 0.22, respectively, for reflections between 9 and 2.3 Å resolution (Table 2). The final model contains 2336 non-hydrogen protein atoms, one FAD moiety, one SO₄²⁻, and 332 solvent molecules. The atomic coordinates of the Arg264Glu FNR mutant have been deposited in the Protein Data Bank (code 1bjk).

RESULTS

Expression and Purification of Arg100Ala and Arg264Glu FNR Mutants. The level of expression in *E. coli* of Arg100Ala and Arg264Glu *Anabaena* PCC 7119 FNR mutants was judged to be similar to that of the recombinant wild-type enzyme. Both mutants were purified by following the same protocol as for the wild-type FNR. The Arg100Ala FNR mutant was found to interact weakly with the Cibacron-Blue Sepharose matrix. Proteins were obtained in homogeneous form, as shown by SDS-PAGE.

Spectral Properties. No major differences were detected in the UV-visible, FAD and protein fluorescence, and circular dichroism spectra of the Arg100Ala and Arg264Glu FNR mutants compared to those of the wild-type FNR (not shown). These data indicate that no major structural perturbations have taken place upon replacement of Arg100 by alanine and Arg264 by glutamic acid in *Anabaena* PCC 7119 FNR.

Steady-State Kinetics. The steady-state catalytic behaviors of the Arg100Ala and Arg264Glu FNR mutants were determined for two reactions catalyzed by FNR. All the kinetic parameters were obtained by fitting the data to the equation for a ping-pong mechanism. The calculated values are shown in Table 3 and compared with those reported for the wild-type enzyme (11). Only small differences were detected in the *k*_{cat} of either FNR mutant for the diaphorase activity with DCPIP, the values being 70 and 74% of those of the wild-type enzyme, respectively. Nevertheless, the *K*_m value for NADPH of Arg100Ala FNR is 12-fold larger than that of the wild-type enzyme, while only a small increase in this parameter is detected for Arg264Glu FNR. The kinetic parameters indicate that Arg100Ala and Arg264Glu FNR

mutants react with 5 and 41% of the catalytic efficiency of wild-type FNR, respectively, when assaying the diaphorase activity with DCPIP.

The NADPH-dependent cytochrome *c* reductase activity of these two FNR forms was studied using either ferredoxin or flavodoxin as the mediator. No changes were detected in the catalytic constants for these two mutants, either with ferredoxin or with flavodoxin (Table 3). Nevertheless, these replacements caused different effects on the *K*_m values obtained for the different FNR substrates. Arg100Ala FNR showed a *K*_m value for NADPH 46 times larger than that reported for wild-type FNR, while only minor changes were detected in this parameter for the protein electron acceptors ferredoxin and flavodoxin. This indicates that for this mutant, the catalytic efficiency with NADPH is only 2% of that of the wild-type enzyme, whereas the mutant is still able to transfer electrons efficiently to ferredoxin and flavodoxin. The opposite behavior with regard to the *K*_m value is observed when Arg264 is replaced by glutamic acid. This mutant has a *K*_m for NADPH close to that found for the wild-type enzyme, while the corresponding values for ferredoxin or flavodoxin are increased by large factors, thus making the catalytic efficiencies of this mutant only 5 and 6% of that of the wild type when ferredoxin and flavodoxin, respectively, are used in this function.

Interaction of Arg100Ala and Arg264Glu FNR_{ox} with Their Substrates in the Oxidized State. The constants for binding of each mutated FNR_{ox} form to each of its substrates (NADP⁺, ferredoxin, and flavodoxin) were evaluated using difference absorption spectroscopy (11, 15). The spectral changes produced when Arg100Ala and Arg264Glu FNR_{ox} forms were titrated with Fd_{ox} or Fld_{ox} were similar to those found for wild-type FNR (not shown). Moreover, only small changes were observed in the binding properties (Table 4) for both substrates, with the dissociation constants being within a factor of 3 of those of the wild-type enzyme. Only a very small difference in the extinction coefficient was found for the complex formed between Arg264Glu FNR_{ox} and Fld_{ox} (Table 4). The significance of this is unclear.

The spectral perturbations produced when NADP⁺ binds to Arg100Ala and Arg264Glu FNR_{ox} mutants were similar to those found when it binds to wild-type FNR (not shown). Nevertheless, important changes are detected in the dissociation constant and binding energy of Arg100Ala FNR for this substrate with respect to the values reported for the wild-type enzyme (Table 4). The dissociation constants and the binding free energy for the NADP⁺-Arg100Ala FNR_{ox} complex are 75-fold higher and 2.5 kcal/mol more positive, respectively, than those found in the complex with the wild-type enzyme. The corresponding values for the NADP⁺-Arg264Glu FNR_{ox} complex were just 6-fold higher and 1 kcal/mol more positive, respectively. The above results indicate that while the Fd and Fld binding sites in both FNR mutants were only slightly influenced by the amino acid replacements, the NADP⁺ interaction site was significantly changed, especially when Arg100 was replaced by an alanine.

Reduction of Arg100Ala and Arg264Glu FNR Forms Studied by Laser Flash Photolysis. Reduction of Arg100Ala and Arg264Glu FNR mutants by laser-generated dRFH* was monitored by the absorbance decrease at 465 nm, corresponding to FAD reduction. Transients were well fitted by monoexponential curves, and the measured rate constants

Table 3: Steady-State Kinetic Parameters of Wild-Type FNR and the FNR Mutants Arg100Ala and Arg264Glu^a

Diaphorase Activity with DCPIP			
FNR form	k_{cat} (s ⁻¹)	$K_{\text{m}}^{\text{NADPH}}$ (μM)	$k_{\text{cat}}/K_{\text{m}}^{\text{NADPH}}$ (μM ⁻¹ s ⁻¹)
wild type ^b	81.5 ± 3	6.0 ± 0.6	13.5 ± 0.5
Arg100Ala	54.2 ± 0.6	74 ± 3	0.74 ± 0.16
Arg264Glu	60.0 ± 1.5	10.3 ± 0.8	5.6 ± 0.2

NADPH-Dependent Cytochrome <i>c</i> Reductase Activity								
with ferredoxin as the mediator					with flavodoxin as the mediator			
FNR form	k_{cat} (s ⁻¹)	$K_{\text{m}}^{\text{NADPH}}$ (μM)	$k_{\text{cat}}/K_{\text{m}}^{\text{NADPH}}$ (μM ⁻¹ s ⁻¹)	K_{m}^{Fd} (μM)	$k_{\text{cat}}/K_{\text{m}}^{\text{Fd}}$ (μM ⁻¹ s ⁻¹)	k_{cat} (s ⁻¹)	$K_{\text{m}}^{\text{Fld}}$ (μM)	$k_{\text{cat}}/K_{\text{m}}^{\text{Fld}}$ (μM ⁻¹ s ⁻¹)
wild type ^b	200 ± 10	6.0 ± 0.5	33.3 ± 1.7	11 ± 2	18.2 ± 1.0	23.3 ± 1.6	33 ± 5	0.70 ± 0.05
Arg100Ala	200 ± 11	275 ± 17	0.72 ± 0.09	11 ± 2	18.2 ± 1.0	28.3 ± 2.2	78 ± 11	0.36 ± 0.08
Arg264Glu	200 ± 33	7.8 ± 1.2 ^c	25.7 ± 0.2 ^c	212 ± 2	0.98 ± 0.04	21.6 ± 6.0	544 ± 60	0.04 ± 0.005

^a All the reactions were carried out in 50 mM Tris-HCl (pH 8.0) at 25 °C. Unless otherwise stated, when the K_{m} for one FNR substrate is calculated, the other one is present at a saturating concentration. ^b Data from ref 11. ^c Calculated at a nonsaturating ferredoxin concentration (50 μM).

Table 4: Dissociation Constants and Free Energy for Complex Formation of Different *Anabaena* PCC 7119 FNR Forms with NADP⁺, Oxidized Ferredoxin, and Oxidized Flavodoxin^a

FNR form	$K_{\text{d}}^{\text{NADP}^+}$ (μM)	$\Delta\epsilon_{(480-394)}^{\text{NADP}^+}$ (mM ⁻¹ cm ⁻¹)	$\Delta G^{\circ\text{NADP}^+}$ (kcal mol ⁻¹)	K_{d}^{Fd} (μM)	$\Delta\epsilon_{(462)}^{\text{Fd}}$ (mM ⁻¹ cm ⁻¹)	$\Delta G^{\circ\text{Fd}}$ (kcal mol ⁻¹)	$K_{\text{d}}^{\text{Fld}}$ (μM)	$\Delta\epsilon_{(465)}^{\text{Fld}}$ (mM ⁻¹ cm ⁻¹)	$\Delta G^{\circ\text{Fld}}$ (kcal mol ⁻¹)
wild type	5.7 ± 0.3	1.20 ± 0.01	-7.10 ± 0.05	4 ± 1	2.00 ± 0.08	-7.3 ± 0.2	3 ± 1	1.4 ± 0.1	-7.5 ± 0.3
Arg100Ala	423 ± 35	0.65 ± 0.02	-4.58 ± 0.05	10 ± 2	1.92 ± 0.11	-6.8 ± 0.1	3.4 ± 1.0	1.1 ± 0.04	-7.4 ± 0.3
Arg264Glu	34.3 ± 3.8	1.48 ^b ± 0.05	-6.06 ± 0.06	3.3 ^c ± 1.0	1.65 ^c ± 0.08	-7.5 ± 0.2	9.4 ± 5.0	0.3 ± 0.04	-6.8 ± 0.3

^a All the difference spectra were recorded in 50 mM Tris-HCl (pH 8.0) at 25 °C. All the proteins were in the oxidized state. ^b $\Delta\epsilon_{(356-394)}^{\text{NADP}^+}$. ^c Dissociation constant obtained in 4 mM potassium phosphate and 1 mM EDTA (pH 7.0).

Table 5: Kinetic Parameters for Electron Transfer from Reduced Ferredoxin to the Different *Anabaena* PCC 7119 FNR Forms Studied by Laser Flash Photolysis^a

FNR form	reduction by dRFH [*]		reduction by Fd _{rd}	
	$k \times 10^8$ (M ⁻¹ s ⁻¹)	k_{et} (s ⁻¹)	k_{et} (s ⁻¹)	K_{d} for Fd _{rd} -FNR _{ox} (μM) ^b
wild type ^c	2.3 ± 0.1	6200 ± 400	9.3 ± 0.7	
Arg100Ala	3.7 ± 0.1	6000 ± 500	9.6 ± 0.7	
Arg264Glu	1.3 ± 0.1	4200 ± 400	20 ± 2	

^a Values for reduction by Fd_{rd} were obtained from the data in Figure 2 as described in the text. $T = 25$ °C. All samples were prepared in 4 mM potassium phosphate and 1 mM EDTA (pH 7.0). The ionic strength was adjusted to 100 mM using aliquots of 5 M NaCl. ^b These values have not been corrected for the concentration of the preformed complex. ^c Taken from ref 31.

were within a factor of 2 of that determined for wild-type FNR (Table 5), indicating that the FAD of these mutants is accessible and redox active.

The dependencies of k_{obs} on FNR concentration for the Fd-FNR electron-transfer interaction at 100 mM ionic strength for wild-type FNR and the Arg100Ala and Arg264Glu FNR mutants are shown in Figure 2A. The results for the Arg100Ala mutant and wild-type FNR are essentially identical, whereas the result for the Arg264Glu mutant is clearly different. The K_{d} value for the intermediate Fd_{rd}-FNR_{ox} complex and the k_{et} derived from these plots are given in Table 5. It is evident that the k_{et} values for the interaction of the wild type and Arg100Ala with Fd_{rd} are the same within experimental error. The K_{d} value for the intermediate Fd_{rd}-FNR_{ox} complex for the charge-reversal mutant, Arg264Glu, is 2 times larger than for wild-type FNR. Note that these data have not been corrected for the presence of preformed complex. We have previously shown (31) that this correction

has insignificant effects on k_{et} , but does significantly decrease the values of K_{d} without changing their relative values.

Figure 2B shows the dependence of k_{obs} on ionic strength. It is clearly evident that Arg100Ala reacts in a manner essentially identical to that of wild-type FNR. The maximal k_{obs} value obtained for Arg264Glu occurs at a significantly lower ionic strength than for wild-type FNR, which suggests that electrostatic interactions in this charge-reversal mutant have been weakened, which results in electron-transfer-favorable interprotein orientations being more easily accessed at lower ionic strengths.

Reduction Potentials. At similar FNR concentrations, Arg100Ala and Arg264Glu reoxidized Fd_{rd} to essentially the same extent as did wild-type FNR. We interpret this as an indication that the one-electron reduction potentials (E°) of these mutants for the oxidized/semiquinone couple are not appreciably perturbed.

Stopped-Flow Studies of the FNR Mutants Arg100Ala and Arg264Glu. Stopped-flow kinetic studies were carried out for Arg100Ala and Arg264Glu *Anabaena* PCC 7119 FNR forms to further investigate the behaviors observed above. This technique allows us to study the time course of association and electron transfer between FNR, in the oxidized and reduced states, and its NADP⁺/NADPH cofactors as well as its two electron-transfer protein partners, ferredoxin and flavodoxin (11). The kinetics of reduction of *Anabaena* FNR forms by NADPH and the reoxidation of the reduced enzyme by NADP⁺ were determined by following the flavin and the NADP⁺/NADPH spectral changes at 460 and 340 nm, respectively, under anaerobic conditions (11). Reaction of Arg100Ala FNR with NADPH showed a decrease in absorbance at 340 nm, and a decrease at 460 nm, which was best fitted to a first-order equation with an observed rate constant, 11 ± 1 s⁻¹, considerably smaller than

Table 6: Fast Kinetic Parameters for Electron-Transfer Reactions of the Different *Anabaena* PCC 7119 FNR Forms Studied by Stopped-Flow Methods^a

FNR form	k_{obs} (s ⁻¹)			k_{obs} (s ⁻¹)		
	FNR _{ox} with NADPH ^c	FNR _{ox} with Fd _{rd} ^d	FNR _{ox} with Fld _{rd} ^e	FNR _{rd} with NADP ⁺ ^c	FNR _{rd} with Fd _{ox} ^d	FNR _{rd} with Fld _{ox} ^e
wild type ^g	> 600 ^b > 140 ^f	nd ^b 250 ^f ± 30	nd ^b	> 600 ^b	nd ^b	2.5 ± 1.0 1.0 ± 1.0
Arg100Ala	11 ± 1	nd ^b	> 300 ^f 18 ± 5	38 ± 3	nd ^b	5 ± 2 1.5 ± 0.3
Arg264Glu	nd ^b 220 ^f ± 31	nd ^b 161 ± 10	14.6 ± 0.4 3.1 ± 0.2	> 350 ^f	> 200	1.0 ± 0.2 0.75 ± 0.5

^a All the reactions were carried out in 50 mM Tris-HCl (pH 8.0) at 13 °C. The samples were mixed in the stopped-flow spectrometer at the indicated concentrations and redox states. Two values of k_{obs} are given for processes showing double exponentials. ^b Reaction occurred within the instrumental dead time. ^c Reaction followed at 460 nm. ^d Reaction followed at 507 nm. ^e Reaction followed at 600 nm. ^f Most of the reaction took place within the instrumental dead time. ^g Taken from ref 11.

the two rate constants reported for the same reaction of the wild-type enzyme (Figure 3A and Table 6). However, the reaction of Arg264Glu FNR with NADPH showed a behavior similar to that reported for the wild-type enzyme (Table 6), i.e., a fast phase corresponding to charge-transfer complex formation followed by a slower phase ascribed to flavin reduction (11, 41). The very low reactivity of the Arg100Ala mutant with NADPH under our stopped-flow experimental conditions allowed a more detailed study of this process by analyzing the observed rate constants obtained at different NADPH concentrations (Figure 3B). The hyperbolic behavior shown in Figure 3B allowed the data to be fit using the analytical solution (32) of the differential equations describing the two-step mechanism:



From this procedure, K_d for the formation of the intermediate complex can be calculated, as well as the value for the limiting rate constant, k_{et} . These values were $210 \pm 10 \mu\text{M}$ and $86 \pm 6 \text{ s}^{-1}$, respectively. Thus, the free energy for complex formation between NADPH and FNR_{ox} is -5.1 kcal/mol .

The reaction of FNR_{rd} with NADP⁺ was also studied by stopped-flow spectrophotometry (Figure 4A). Increases in absorbance at 460 nm due to FNR reoxidation and at 340 nm due to NADPH formation (not shown) were detected for both mutants, as reported for wild-type FNR (11). Nevertheless, although most of the reoxidation of Arg264Glu FNR took place during the instrumental dead time (Table 6), as was the case for the wild-type enzyme, the observed rate constant for reoxidation of Arg100Ala FNR by NADP⁺ was only $38 \pm 3 \text{ s}^{-1}$ (Table 6 and Figure 4A). The low reactivity of the Arg100Ala FNR_{rd} with NADP⁺ allowed a more detailed study of the process by analyzing the observed rate constants obtained at different NADP⁺ concentrations (Figure 4B). Again, the hyperbolic behavior shown in Figure 4B allowed the data to be fit using the analytical solution (32) of the differential equations describing the two-step mechanism, which in this case is

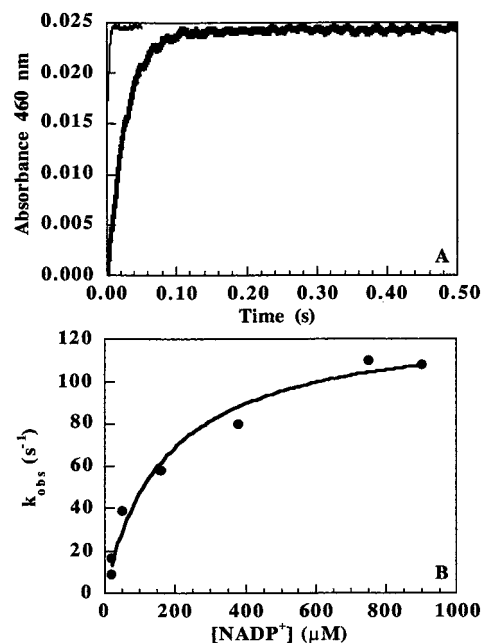
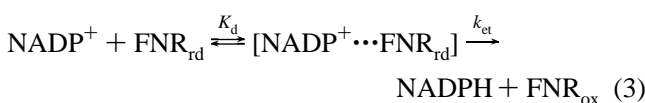


FIGURE 4: (A) Time course of anaerobic reduction of NADP⁺ by FNR_{rd} species. Final concentrations after mixing were as follows: 7.5 μM wild-type FNR_{rd} (narrow trace) was reacted with 44 μM NADP⁺, and 10 μM Arg100Ala FNR_{rd} (wide trace) was reacted with 50 μM NADP⁺. The monitoring wavelength was 460 nm. (B) NADP⁺ concentration dependence of the observed rate constants for Arg100Ala FNR_{rd} reoxidation. Reactions were carried out in 50 mM Tris-HCl (pH 8.0) at 13 °C.

The K_d value for the formation of the intermediate complex is $87.8 \pm 1.0 \mu\text{M}$, and the limiting rate constant, k_{et} , is $128 \pm 20 \text{ s}^{-1}$. The free energy for complex formation between NADP⁺ and FNR_{rd} is -5.2 kcal/mol , which is essentially the same as that obtained for the NADPH–FNR_{ox} complex.

Reactions between FNR and Fd were followed at 507 nm. This wavelength is an isosbestic point for FNR_{ox} and FNR_{sq}, near an isosbestic point for FNR_{sq} and FNR_{rd}, and is appropriate for following reduction or reoxidation of ferredoxin (42). Previous stopped-flow studies of the electron-transfer process between Fd_{rd} and FNR_{ox} have shown that the k_{obs} for electron transfer from Fd_{rd} to wild-type FNR_{ox} producing FNR_{sq} and Fd_{ox} (at least 1000 s^{-1}) must be short enough that the reaction takes place within the instrumental dead time and that the rate constant observed by stopped-flow methods (250 s^{-1} ; Table 6) must correspond to the reoxidation of a second Fd_{rd} molecule and reduction of FNR_{sq} to FNR_{rd} (11, 41). Reduction of Arg100Ala FNR by Fd_{rd}

could not be followed under our experimental conditions by stopped-flow methods, indicating that the processes involving this reaction occurred within the instrumental dead time, and thus that it behaves in a manner very similar to that of the wild-type protein. However, when the reaction of Arg264Glu FNR_{ox} with Fd_{rd} was analyzed by stopped-flow methods, although the rate constant for reduction of the protein by Fd_{rd}, as expected from the obtained laser flash photolysis data, is still too fast to be detected, a significant decrease is obtained in the k_{obs} value for the reduction of the FNR_{sq} previously formed by a second Fd_{rd} molecule (Table 6).

Reduction of ferredoxin by the Arg100Ala and Arg264Glu FNR_{rd} forms was also assayed. In all cases, the data collected for the stopped-flow reaction were best fit to a single-exponential equation (Table 6), as was the case for the wild-type enzyme (11). This process, which was too fast to be followed by stopped-flow spectrophotometry for the wild-type FNR (11), was also too fast to be detected for Arg100Ala FNR_{rd}. However, when reduction of ferredoxin by Arg264Glu FNR_{rd} was studied, although near the instrumental dead time, we were able to detect a decay which corresponded to a rate constant of $>200 \text{ s}^{-1}$, demonstrating that this process has been affected by the mutation, although we were not able to quantitate it.

Electron-transfer reactions between FNR and flavodoxin were also analyzed for the Arg100Ala and Arg264Glu FNR mutants by stopped-flow methods, and the results were compared with those reported for the wild-type enzyme (11). As previously described, the time course of wild-type FNR_{ox} reduction by reduced flavodoxin cannot be followed by stopped-flow methods (11). Nevertheless, the Arg100Ala and Arg264Glu FNR forms produced traces for this reaction that could be analyzed and which were best fit by a two-exponential equation (not shown). Reduction of Arg100Ala FNR_{ox} by Fld_{rd} took place with a rapid rate constant of $>300 \text{ s}^{-1}$ and a smaller rate constant of 18 s^{-1} . Both phases had similar amplitudes. The rate constant of the fast reaction is consistent with the formation of both semiquinones, being in the range observed for wild-type FNR. The second, slower, reaction, which was not detected for wild-type FNR (11), could be due to the reduction of FNR_{sq} to the fully reduced state by a second molecule of Fld_{rd}. This result indicates that replacement of Arg100 by alanine produced an enzyme with properties for accepting electrons from reduced Fld slightly altered compared to those of wild-type FNR.

When the electron-transfer process from Fld_{rd} to Arg264Glu FNR_{ox} was studied, two different phases were also observed (not shown). However, in this case, both observed rate constants were considerably smaller than those obtained for the reduction of the wild-type enzyme by Fld_{rd} (Table 6). Thus, replacement of Arg264 by a glutamic acid residue produced an enzyme which was highly impaired in its ability to accept electrons from Fld_{rd}, with observed rate constants of 14.6 and 3.1 s^{-1} for the two processes involved in the electron-transfer reaction, i.e., formation of two semiquinone molecules followed by reduction of one FNR_{sq} to FNR_{rd} by a second Fld_{rd} molecule, respectively.

The electron-transfer reaction from FNR_{rd} to Fld_{ox} was also analyzed for both FNR mutants. As reported previously (11) for the electron transfer from wild-type FNR_{rd} to Fld_{ox}, two phases for the process were also detected for the Arg100Ala and Arg264Glu FNR mutants (Table 6). These phases cor-

responded, as previously proposed, to the processes of electron transfer from FNR_{rd} to Fld_{ox} for producing FNR_{sq} and Fld_{sq}, followed by reduction of a second molecule of Fld_{ox} to the semiquinone state by FNR_{sq} (11). Arg100Ala FNR behaves in a manner quite similar to that of the wild-type enzyme (Table 6; the larger k_{obs} value obtained for this mutant is due to the use of 50% more Arg100Ala FNR in this assay). The rate constants obtained for the reaction when Arg264Glu FNR_{rd} is the electron donor to Fld_{ox} appear to be between 40 and 75% of those reported for the wild-type enzyme (Table 6), indicating that, although altered, this process is also still efficient for this mutant.

To determine if the reoxidation of the Arg100Ala and Arg264Glu mutants by molecular oxygen followed a process similar to that of the wild-type enzyme, flavin reoxidation by molecular oxygen was followed by stopped-flow spectrophotometry at 460 and 600 nm. Reoxidation of the FAD can be followed at 460 nm, while 600 nm is the wavelength at which the appearance of the neutral flavin semiquinone obtained upon reaction of the fully reduced enzyme with O₂ can be monitored, and the subsequent slower reaction of the semiquinone with a second oxygen molecule. The traces obtained for both FNR mutants (not shown) gave the same profile as those reported for the wild-type enzyme at both wavelengths (11), indicating that the sequence followed in the reoxidation of these FNR_{rd} forms must be similar to that of the native enzyme, producing an intermediate semiquinone state.

Three-Dimensional Structure of the Arg264Glu FNR Mutant. The three-dimensional structure of the Arg264Glu mutant has been obtained by X-ray diffraction. In the three-dimensional model obtained, Glu264 lies on the surface of the FNR molecule near the C-terminal Tyr303 residue (Figure 5A). There are no significant deviations between the mutated and native structures as shown by the low root-mean-square deviations (0.4 \AA) of the C α backbone of the mutant superimposed on the native FNR backbone. The main differences are concentrated in the loop starting at Tyr104 and ending at Val113, but they are not significant due to the poor definition of the electron density map in this region.

Structural differences are also observed in the FAD cofactor which is well fit by the electron density map. The positions of the isoalloxazine ring system and the ribityl chain are well conserved in all three structures thus far reported for *Anabaena* FNR (wild-type FNR, wild-type FNR–NADP⁺, and Arg264Glu FNR), which is consistent with this group being tightly bound to the protein. The rest of the cofactor is similarly ordered in the mutant and in the native structure, with both of them showing the largest differences in the phosphate–ribose moiety of the ADP, as compared to the wild-type FNR–NADP⁺ complex. However, if the large distance between the FAD and the NADP⁺ is taken into account, these differences do not correlate with the extent of NADP⁺ binding and are supposedly a consequence of the FAD chain flexibility. The Glu264 residue is well defined in the electron density map (Figure 5B), although some chain mobility is detected as shown by the high thermal atomic factors. The maximum B value exhibited by the carboxylic oxygen is 61 \AA^2 . The Arg can adopt two different conformations in the wild-type FNR structure, depending on whether the NADP⁺ cofactor is bound. The side chain conformation of the Glu264 residue is similar to the Arg conformation

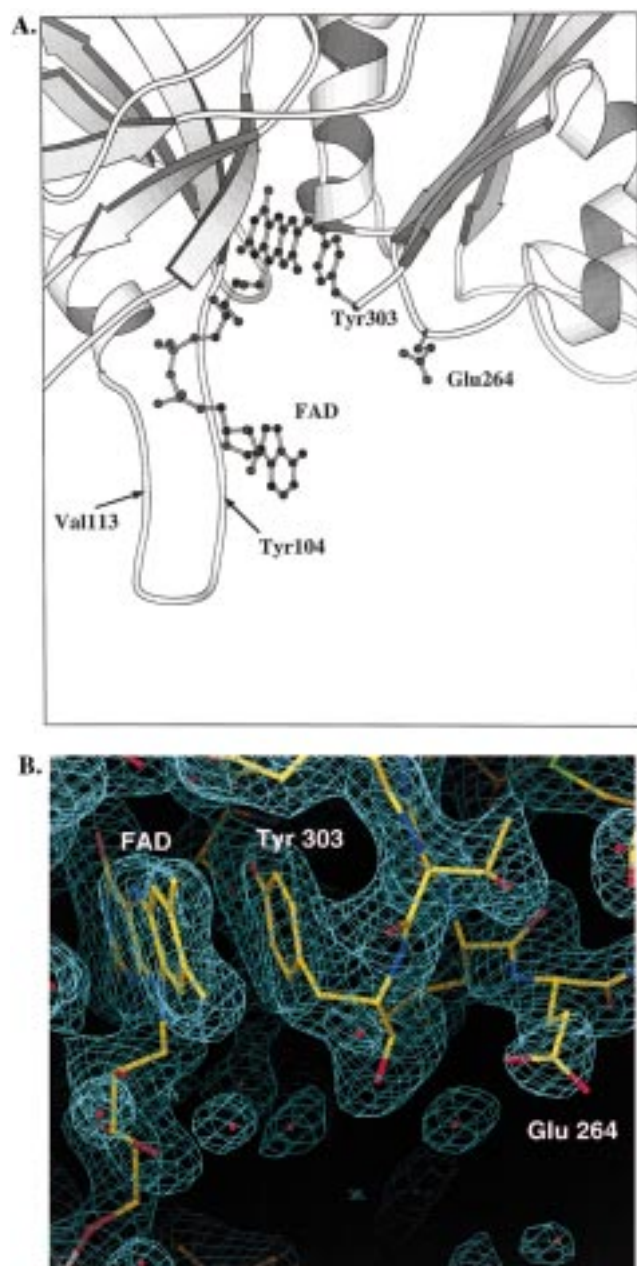


FIGURE 5: (A) MOLSCRIPT drawing (54) of the *Anabaena* PCC 7119 Arg264Glu FNR mutant showing the secondary structure elements in the region of the mutation. The FAD cofactor and residues Tyr303 and Glu264 are shown as balls and sticks. (B) A $2F_o - F_c$ electron density map of the Arg264Glu FNR form in the vicinity of the mutated residue. The map was contoured at 1σ . The figure was generated with the graphics program O (40).

found in the wild-type FNR–NADP⁺ complex. As a consequence, one of the carboxylic oxygens of Glu is situated near the position of the N ϵ of the guanidinium portion of the Arg residue. However, neither the Arg N ϵ nor the Glu O ϵ is involved in any hydrogen bond, and therefore, the side chain of this residue does not seem to play a critical role in the stabilization of the proximal C-terminal Tyr303. This fact is confirmed by the two different conformations of Arg264, despite the large distance between this residue and the NADP⁺ molecule in the crystal. The NH₂ group of Arg264 is hydrogen bonded to the carboxylate of Tyr303 in the same side chain conformation observed in the wild-type FNR–NADP⁺ complex, but this only provides a more ordered Arg as shown by the smaller temperature factors of this residue

in the crystal. The stabilization of the main chain at the C-terminal Tyr303 is most likely due to the strong hydrogen bond between the backbone atoms NH(303)···CO(262) that is absolutely conserved in all three structures.

DISCUSSION

As noted in the introductory section, although attempts to crystallize FNR in a complex with NADP⁺ have been made (2, 4, 5), thus far there is no crystallographic three-dimensional structure for a functional FNR–NADP⁺ complex. The only available structure of a complex shows the nicotinamide ring of NADP⁺ and the isoalloxazine ring of the FAD far away from each other and therefore in an apparently nonfunctional orientation (5). As a consequence, only modeled complexes based upon the known crystal structures of the protein and various biochemical data are available (5, 12, 13, 19, 20, 43). Chemical modification studies have demonstrated the important role of Arg100 from *Anabaena* PCC 7119 FNR, and the corresponding Lys116 in the spinach enzyme, in NADP⁺ binding (12–14, 17, 19). These results are completely consistent with the crystal structures obtained to date. Arg100 extends from the FAD domain to make a hydrogen bond with the 5'-phosphate, although it is not clear which part of the pyrophosphate it will interact with in a functional complex (5, 43). Furthermore, a role in NADP⁺ binding has also been ascribed to Arg264 (5), and the importance of a positive charge at this position in the *Anabaena* enzyme in its interaction with ferredoxin has also been suggested (23). In this paper, we probe the importance of these residues in the *Anabaena* enzyme. The positive charge and the long side chain of Arg100 have been replaced by an alanine, while a charge-reversal mutation, from Arg to Glu, was made at Arg264. The anomalous behavior of the Arg100Ala mutant on the affinity chromatography column (see the Results) seems to correlate with the decrease in affinity for NADP⁺. Spectroscopic characterization did not reveal major differences in either mutant, indicating that gross protein structural rearrangements did not occur upon mutation.

The residue in the spinach enzyme, Lys116, which corresponds to Arg100 has previously been studied by site-directed mutagenesis (20), in which a glutamine residue was introduced at that position, preserving the ability to form hydrogen bonds while removing the net positive charge. The results presented here complement that study, since we have removed the positive charge, the steric hindrance due to the long side chain, and the ability to make hydrogen bonds. We have found that replacing Arg100 with an alanine in *Anabaena* PCC 7119 FNR produced an enzyme which had only 13% of the catalytic efficiency of the wild-type FNR (Table 3) in the diaphorase assay with DCPIP. However, replacement of the equivalent residue in the spinach FNR with glutamine caused more drastic changes in the diaphorase activity. The catalytic efficiency of this enzyme was only 0.2% of that of the wild-type spinach FNR (20). When the behavior of the Arg100Ala mutant in the NADPH dependent cytochrome *c* reductase activity was studied, either with ferredoxin or with flavodoxin, no changes were detected in the k_{cat} and K_m values for Fd, and in the K_m value for Fld, with respect to those of the wild-type enzyme. However, the catalytic efficiency for NADPH was reduced to 2% of that of the wild-type enzyme, in accordance with the diaphorase

activity data. The dissociation constant values obtained for the Arg100Ala FNR_{ox} complex either with Fd_{ox} or with Fld_{ox}, as studied by difference spectroscopy (Table 4), and of the Fd_d–Arg100Ala FNR_{ox} complex, as studied by laser flash photolysis (Table 5), showed that this residue is not crucial in ferredoxin or flavodoxin recognition. However, a 75-fold increase of the dissociation constant is observed for NADP⁺, as well as a decrease in the difference extinction coefficient, indicating the importance of this residue in NADP⁺ binding to FNR. Moreover, the low reactivity of this mutant observed by stopped-flow spectrophotometry with NADP⁺/NADPH allowed the calculation of the dissociation constants and the free energies for the intermediate complexes, NADPH–FNR_{ox} and NADP⁺–FNR_{rd}. The K_d value obtained was much larger than that for the reaction of wild-type FNR, and the free energy for complex formation was considerably smaller than that for the wild-type enzyme. No significant difference spectrum was detected in the case of the spinach Lys116Gln FNR mutant when it was titrated with NADP⁺ (20). Therefore, replacement of Lys116 by Gln in spinach FNR produced an enzyme which had a much lower affinity for NADP⁺ than the mutation made in *Anabaena*, where the equivalent position has been mutated to alanine. Fast electron-transfer kinetics, laser flash photolysis, and stopped-flow experiments confirmed that electron-transfer reactions between FNR and ferredoxin, in both directions, were not affected by the introduced mutation, indicating that Arg100 is not involved in these processes. However, some small differences were found in the reactions of this mutant with flavodoxin, either by steady-state or by stopped-flow methods (Tables 3 and 6). It is known that reactivity between FNR and Fld is not as efficient as expected in some processes, although there is no convincing explanation for this. In this regard, the importance of structural aspects of the proteins participating in electron-transfer processes over thermodynamic factors is assumed (11).

Examination of the structure around Arg100 in *Anabaena* FNR shows that the guanidinium group is fully exposed to the solvent and does not make contact with any other residues, only with water molecules. The same situation is found when the ϵ -NH₂ group of Lys116 in the spinach enzyme is analyzed and a Gln residue is modeled at this position. In both the Ala mutation in *Anabaena* FNR and the Gln mutation modeled in the spinach FNR, the positive charge, which is proposed to be involved in pyrophosphate binding and stabilization, has been removed. Although the Gln residue could still be capable of some stabilization due to its ability to make hydrogen bonds, it is shorter than Lys or Arg and might not extend far enough to adequately stabilize the NADP⁺ pyrophosphate bridge. Moreover, our crystallographic data indicate that the position of the Arg residue is very important for proper orientation of NADP⁺ and that the bulky side chain of the Gln residue in the mutant spinach enzyme might block the nicotinamide from binding appropriately. NADP⁺ may still bind to the protein, as was the case in the *Anabaena* crystals, but not with the proper orientation for its catalytic function (Figure 1) (5). However, in the alanine mutant, the side chain is considerably shortened, thereby avoiding any steric hindrance. In this case, we can expect to have NADP⁺ binding, but to a lesser extent than for the wild-type enzyme. These results confirm the fact that the side chain of Arg100 in *Anabaena* (and Lys116

in spinach) FNR plays a key role in the binding and proper orientation of NADP(H) in the ground and transition states.

With regard to Arg264 of *Anabaena* FNR, the results show that the reactions of the enzyme with NADP⁺/NADPH were only slightly affected when this residue was replaced by Glu. The slightly higher dissociation constant obtained for the NADP⁺–Arg264Glu FNR_{ox} complex might account for the observed changes in reactivity. These results could still be consistent with Arg264 in the FNR enzyme playing the proposed role (5) of interacting with the C-terminal tyrosine, moving it in such a way as to enable the nicotinamide of NADP⁺ to bind at that position. A glutamate residue (this work) or a lysine residue present in other FNR sequences (Table 1) could substitute for arginine to provide such stabilization. However, due to the different length of the Glu side chain as compared to the Arg side chain, modeling of the carboxylate group stacked with Tyr aromatic ring is not possible in the three-dimensional structure obtained for the mutant. Therefore, we conclude that the glutamic acid residue would not be able to provide the necessary movement of the terminal Tyr, thereby enabling NADP⁺ binding at this position. Considering that the ability to bind NADP⁺ is essentially unaffected by the mutation at this site, we assume that the role assigned to this Arg in Tyr303 stabilization is not critical.

Altered characteristics have been observed for the Arg264Glu mutant in its reactions with its protein partners, ferredoxin and flavodoxin (Tables 2 and 5). Although the dissociation constants, obtained either by difference spectroscopy or by laser flash photolysis, differ by a factor of 2 from those obtained for the wild-type enzyme (Tables 4 and 5), even larger increases are observed for the K_m values obtained in the NADPH-dependent cytochrome *c* reductase activity, either for ferredoxin or for flavodoxin. The reactions with both mediators are 20 times less efficient than those obtained using wild-type FNR (Table 3). On the other hand, when the fast kinetic reactions between FNR and Fd were studied, either by laser flash photolysis or by stopped-flow methods, only minor decreases in k_{et} and k_{obs} were obtained (Tables 5 and 6). However, the ionic strength behavior observed for Arg264Glu FNR (Figure 2B) suggests that electrostatic interactions in this charge-reversal mutant have been weakened, which results in electron-transfer-favorable interprotein orientations being accessed more easily at lower ionic strengths. The most drastic effect is observed in the reaction of this mutant with Fld_d, where the observed rate constant for transfer of one electron from Fld_d to the mutant is much smaller than that for the wild-type enzyme. In contrast, one of the observed rate constants obtained for the reaction of Arg264Glu FNR_{rd} with Fld_{ox} is 2.5 times smaller than and the other is the same, within experimental error, as those obtained for the wild-type enzyme.

It has been suggested that a series of basic residues located in one region of the FNR surface (23), as shown in Figure 6A, interact with acidic residues on Fd to form the interface of the FNR–ferredoxin complex. Careful inspection of the structure suggests a prominent role for Lys72, Lys75, and Arg264 in aligning the [2Fe-2S] cluster of ferredoxin with the FAD moiety of FNR, due to the proximity of these residues to the cofactor. The change of polarity in the FAD environment introduced by the Arg264Glu mutation (Figure 6B) must have a marked destabilizing effect on the complex

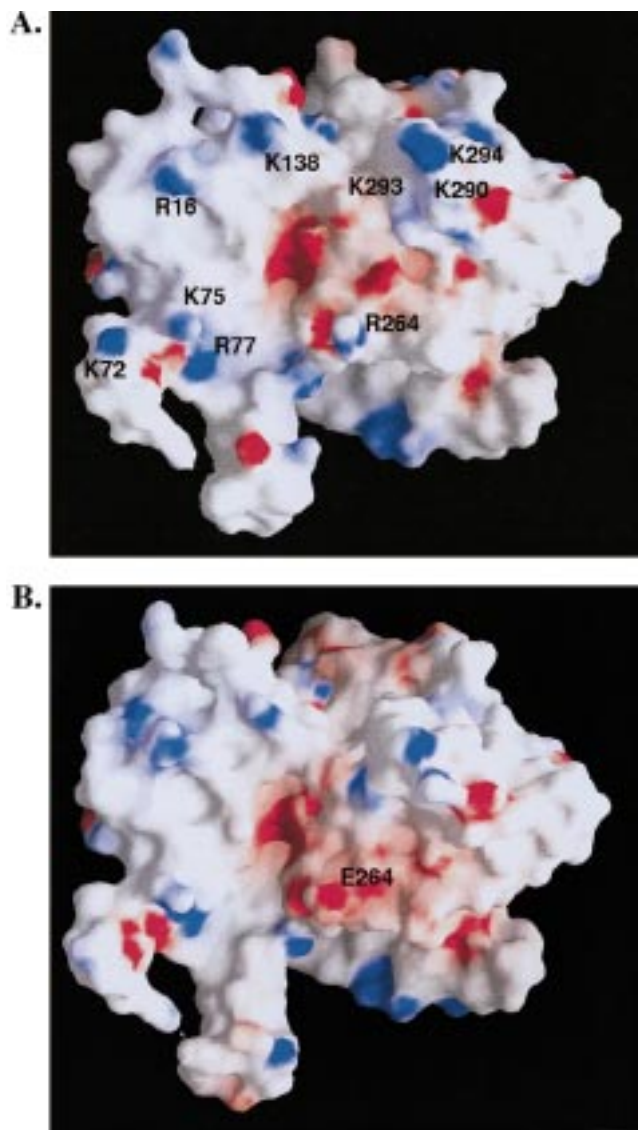


FIGURE 6: Molecular surface showing electrostatic surface potentials of (A) wild-type FNR and (B) Arg264Glu FNR. Positive potential is shown in blue and negative potential in red. The FAD cofactor is not included. The figure was generated with GRASP (55).

since electrostatic interactions are an important component of the complex interface. It is important to note that the shorter Glu side chain does not protrude from the FNR surface, although replacement of Arg264 by glutamic acid produced a completely different charge distribution around the proposed binding site for ferredoxin, in a region close to the flavin isoalloxazine ring (Figure 6). The presence of such negative charge does not completely preclude complex formation or electron transfer with the FNR protein partners but, in the case of the ferredoxin reaction, seems to produce a slightly weaker complex which more easily rearranges to its optimal conformation. However, the data obtained with stopped-flow methods indicate that this same effect does not occur in the interaction of Fld_{rd} with Arg264Glu FNR_{ox}, where some specific structural feature of reduced flavodoxin likely produces an electrostatic repulsion of the negative charge introduced on FNR.

The crystallographic results clearly demonstrate that structural alterations in the immediate vicinity of the mutation do not occur, and although some perturbations in the loop

of Tyr104–Val113 and in the adenine group of the FAD have been observed, these changes do not correlate with NADP⁺ binding. Thus, differences observed in reactivity with the protein partners cannot be attributed to any structural or conformational change caused by the mutated residue. The different charge and mobility of the Arg264 side chain as compared to those of the Glu side chain may explain differences in reactivity, thereby indicating that this residue may be involved in the orientation of the proteins, allowing the prosthetic groups to interact properly during FNR–ferredoxin (–flavodoxin) complex formation.

In conclusion, the results of this study reveal important new conceptual information about the interaction of FNR with its substrates. A critical role is confirmed for the long side chain and positive charge of Arg100 in the *Anabaena* PCC 7119 FNR. Studies on the Arg264Glu FNR mutant establish that the Arg264 side chain is not required for the proper orientation of the nicotinamide or for its interaction with the isoalloxazine portion of the FAD. However, its charge properties influence the interaction with Fd during complex formation prior to electron transfer.

REFERENCES

- Serrano, A., Rivas, J., and Losada, M. (1984) *FEBS Lett.* 170, 85–88.
- Bruns, C. M., and Karplus, P. A. (1995) *J. Mol. Biol.* 247, 125–145.
- Correll, C. C., Ludwig, M. L., Bruns, C. M., and Karplus, P. A. (1993) *Protein Sci.* 2, 2112–2133.
- Karplus, P. A., Daniels, M. J., and Herriott, J. R. (1991) *Science* 251, 60–66.
- Serre, L., Vellieux, F. M. D., Medina, M., Gómez-Moreno, C., Fontecilla-Camps, J. C., and Frey, M. (1996) *J. Mol. Biol.* 263, 20–39.
- Hurley, J. K., Cheng, H., Xia, B., Markley, J. L., Medina, M., Gómez-Moreno, C., and Tollin, G. (1993) *J. Am. Chem. Soc.* 115, 11698–11701.
- Hurley, J. K., Fillat, M. F., Gómez-Moreno, C., and Tollin, G. (1995) *Biochimie* 77, 539–548.
- Hurley, J. K., Medina, M., Gómez-Moreno, C., and Tollin, G. (1994) *Arch. Biochem. Biophys.* 312, 480–486.
- Hurley, J. K., Salamon, Z., Meyer, T. E., Fitch, J. C., Cusanovich, M. A., Markley, J. L., Cheng, H., Xia, B., Chae, Y. K., Medina, M., Gómez-Moreno, C., and Tollin, G. (1993) *Biochemistry* 32, 9346–9354.
- Hurley, J. K., Schmeits, J. L., Genzor, C., Gómez-Moreno, C., and Tollin, G. (1996) *Arch. Biochem. Biophys.* 333, 243–250.
- Medina, M., Martínez-Júlvez, M., Hurley, J. K., Tollin, G., and Gómez-Moreno, C. (1998) *Biochemistry* 37, 2715–2728.
- Medina, M., Méndez, E., and Gómez-Moreno, C. (1992) *FEBS Lett.* 298, 25–28.
- Medina, M., Méndez, E., and Gómez-Moreno, C. (1992) *Arch. Biochem. Biophys.* 299, 281–286.
- Medina, M., Gómez-Moreno, C., and Tollin, G. (1992) *Eur. J. Biochem.* 210, 577–583.
- Sancho, J., and Gómez-Moreno, C. (1991) *Arch. Biochem. Biophys.* 288, 231–233.
- Fillat, M. F., Sandmann, G., and Gómez-Moreno, C. (1988) *Arch. Microbiol.* 150, 160–164.
- Cidara, D., Biondi, P. A., Zanetti, G., and Ronchi, S. (1985) *Eur. J. Biochem.* 146, 295–299.
- Chan, R. L., Carrillo, N., and Vallejos, R. H. (1985) *Arch. Biochem. Biophys.* 240, 172–177.
- Aliverti, A., Gadda, G., Ronchi, S., and Zanetti, G. (1991) *Eur. J. Biochem.* 198, 21–24.
- Aliverti, A., Lübberstedt, T., Zanetti, G., Herrmann, T. G., and Curti, B. (1991) *J. Biol. Chem.* 266, 17760–17763.

21. Pai, E. F., Karplus, P. A., and Schulz, G. E. (1988) *Biochemistry* 27, 4465–4474.
22. Li, R., Bianchet, M. A., Talay, P., and Amzel, M. (1995) *Proc. Natl. Acad. Sci. U.S.A.* 92, 8846–8850.
23. Schmitz, S., Martínez-Júlvez, M., Gómez-Moreno, C., and Böhme, H. (1998) *Biochim. Biophys. Acta* 1363, 85–93.
24. Fillat, M. F., Flores, E., and Gómez-Moreno, C. (1993) *Plant Mol. Biol.* 22, 725–729.
25. Gómez-Moreno, C., Martínez-Júlvez, M., Fillat, M. F., Hurley, J. K., and Tollin, G. (1995) in *Photosynthesis: from Light to Biosphere* (Mathis, P., Ed.) Vol. II, pp 627–632, Kluwer Academic Publishers, Dordrecht, The Netherlands.
26. Fillat, M. F., Borrias, W. E., and Weisbeek, P. J. (1991) *Biochem. J.* 280, 187–191.
27. Avron, M., and Jagendorf, A. T. (1956) *Arch. Biochem. Biophys.* 65, 475–490.
28. Shin, M. (1971) *Methods Enzymol.* 23, 440–442.
29. Przysiecki, C. T., Bhattacharyya, A. K., Tollin, G., and Cusanovich, M. A. (1985) *J. Biol. Chem.* 260, 1452–1458.
30. Tollin, G., Hurley, J. K., Hazzard, J. T., and Meyer, T. E. (1993) *Biophys. Chem.* 48, 259–279.
31. Hurley, J. K., Fillat, M. F., Gómez-Moreno, C., and Tollin, G. (1996) *J. Am. Chem. Soc.* 118, 5526–5531.
32. Simonsen, R. P., and Tollin, G. (1983) *Biochemistry* 22, 3008–3016.
33. Simonsen, R. P., Weber, P. C., Salemme, F. R., and Tollin, G. (1982) *Biochemistry* 21, 6366–6375.
34. Matthews, B. W. (1968) *J. Mol. Biol.* 33, 491–497.
35. Leslie, A. G. W. (1987) in *Proceedings of the CCP4 Study Weekend* (Helliwell, J. R., Machin, P. A., and Papiz, M. Z., Eds.) pp 39–50, SERC Daresbury Laboratory, Warrington, U.K.
36. Collaborative Computational Project Number 4 (1994) *Acta Crystallogr. D* 50, 760–763.
37. Navaza, J. (1994) *Acta Crystallogr. A* 50, 157–163.
38. Castellano, E., Oliva, G., and Navaza, J. (1992) *J. Appl. Crystallogr.* 25, 281–284.
39. Brünger, A. T. (1993) *X-PLOR: A system for X-ray Crystallography and NMR*, Yale University Press, New Haven, CT.
40. Jones, T. A., Zou, J. Y., Cowan, S. W., and Kjeldgaard, M. (1991) *Acta Crystallogr. A* 47, 110–119.
41. Batie, C., and Kamin, H. (1984) *J. Biol. Chem.* 259, 8832–8839.
42. Pueyo, J. J., Gómez-Moreno, C., and Mayhew, S. G. (1991) *Eur. J. Biochem.* 202, 1065–1071.
43. Karplus, P. A., and Bruns, C. M. (1994) *J. Bioenerg. Biomembr.* 26, 89–99.
44. Fillat, M. F., Bakker, H. A. C., and Weisbeek, P. J. (1990) *Nucleic Acids Res.* 18, 7161.
45. Yao, Y., Tamura, T., Wada, K., Matsubara, H., and Kodo, K. (1984) *J. Biochem.* 95, 1513–1516.
46. Michalowski, C. B., Schmitt, J. M., and Bohnert, H. J. (1989) *Plant Physiol.* 89, 817–822.
47. Newman, B. J., and Gray, J. C. (1988) *Plant Mol. Biol.* 10, 511–520.
48. Jakowitsch, J., Bayer, M., Maier, T., Brandtner, M., Hamiton, B., Neumann-Spallart, C., Lutke, A., Michalowski, C. B., Bohnert, H. J., Schenk, H. E. A., and Löfflerhardt, W. (1993) Gen-Bank Accession No. X66732.
49. Schluchter, W. M., and Bryant, D. A. (1992) *Biochemistry* 31, 3092–3102.
50. Haniu, M., McManus, M. E., Birkett, D. J., Lee, T. D., and Shively, J. E. (1989) *Biochemistry* 28, 8639–8645.
51. Ostrowski, J., Barber, M. J., Tueger, D. C., Miller, B. E., Siegel, L. M., and Kredich, N. M. (1989) *J. Biochem. (Tokyo)* 96, 579–582.
52. Yubisui, T., Miyata, T., Iwanaga, S., Tamura, M., Yoshida, S., Takeshita, M., and Nakajima, H. (1984) *J. Biochem.* 96, 579–582.
53. Correll, C. C., Batie, C. J., Ballow, D. P., and Ludwig, M. L. (1992) *Science* 258, 1604–1610.
54. Kraulis, P. J. (1991) *J. Appl. Crystallogr.* 24, 946–950.
55. Nicholls, A., Bharadwaj, R., and Honig, B. (1993) *Biophys. J.* 64, 166.

BI981718I